Mechanism and Machine Theory 44 (2009) 615–632

Contents lists available at ScienceDirect

Mechanism and Machine Theory

journal homepage: www.elsevier.com/locate/mechmt

Modelling and parametric study of modular undulating fin rays for fish robots

K.H. Low

School of Mechanical and Aerospace Engineering, Nanyang Technological University (NTU), Singapore 639798, Republic of Singapore

ARTICLE INFO

Article history:
Received 12 November 2007
Received in revised form 31 October 2008
Accepted 17 November 2008

Keywords:
Biomimetics
Fish robots
Undulating fins
Modular mechanism
Buoyancy tank
Workspace and locomotion

ABSTRACT

Biomimetic robots borrow their senses and structure from animals, such as insects, fish and birds. Development of underwater vehicles is one of the areas where biomimetic robots can potentially perform better than conventional robots. In this paper, the biomimetic design and the workspace study of undulating fin propulsion mechanisms are considered and discussed. We are interested in fish with long and/or wide undulating body/fin – especially those of anguilliform, amiiform, rajiform, and gymnotiform. Two major mechanism layouts developed to mimetic fin undulations of real fish are compared and discussed. Various kinematics expressions of fin waves are presented and the model's limitation is also discussed. For a parametric study, the geometry of a single fin segment of the assembled fin mechanisms and the fin wave generated are first developed. Next, the fin workspace of the single fin segment is derived based on a defined area ratio. By virtue of the obtained fin dimensions, a gymnotiform robot, Nanyang knifefish (NKF-II), has been designed and constructed. With the fin-ray linkages with sliders connecting in series, the fish robot is able to generate arbitrary undulating waveforms. The robot's maneuvering and its depth control have also been achieved by the integration of a buoyancy tank with the undulating fin mechanisms. Initial pool testing has been conducted to demonstrate the basic performance of the fish robot underwater.

1. Introduction

Biomimetic robots borrow their senses and structure from animals, such as insects, fish and birds. It is believed that the bio-inspired systems function better in the unpredictable real world than the controlled artifice of a laboratory. Robotics engineers are able to combine the study and the findings of biology and engineering [1–6], while a group of researchers is actively exploring the lightweight or micro-robotic fish with smart materials for actuation and locomotion [7–9]. Another reason for the focus in biomimetics propulsion means is the increasing awareness to preserve the environment. The marine ecological environment has been deteriorating because of human interaction with them. One extremely destructive tool used by such human interaction is the propeller, the main propulsion systems used by most current water vehicles. The broadband noise from cavitating propellers of any motorized vessel may have severe acoustic effects on marine wildlife, like changes of behaviour, 'masking' of other signals, or causes temporary (or permanent) hearing trauma [10].

The present work is concerned with the design of undulating fins and the parametric study of fin workspace. We first understand the fin propulsion of real fish. The fish we are interested are in those having long and wide undulating body/fin. Fish of undulatory mode generally exhibit more flexible swimming skills, but relatively lower speed over the oscillatory

E-mail address: mkhlow@ntu.edu.sg

0094-114X/$ - see front matter © 2008 Elsevier Ltd. All rights reserved.
doi:10.1016/j.mechmachtheory.2008.11.009

ones. As a typical individual of gymnotiform fish, Black Ghost knifefish swims by the undulation of its long-based anal fin below the body, while the body axis is held straight in many cases. This special morphological structure is generally thought to have advantages in reducing the friction drag in undulatory movements [5].

In this paper, we also present an in-depth study of the modular undulating fin with sliders, which has been implemented by Low and Willy [4]. Moreover, this mechanism is also compared with another undulating fin with a fixed base line and several individual fin rays, separately proposed and designed by Toda [3] or Hu [11].

The rest of the paper is organized as follows. Section 2 reviews the natural fish and its robotic counterpart from the view of biomimetics. In Section 3, we propose a MPF-type undulating fin with sliders. We also present detailed mechanism design and workspace analysis of the proposed mechanism and compared with the other undulating fin mechanisms by a fixed base line. Section 4 focuses on the workspace study of the MPF-type undulating fin and the parametric study is based on a defined "area ratio". We then present a fish robot constructed by integrating a buoyancy tank with the proposed fin segments of dimensions obtained in the parametric study. Finally, the work is concluded with some remarks.

2. Review of natural and biomimetic MPF fish

2.1. Biological median and/or paired fin (MPF)

Classification of the fish is based on two main factors [5,12]: (1) the extend to which propelling process is based on undulatory motion versus oscillatory motion, and (2) the body structures or fin segments that contribute most in generating propulsion. With the classification, fish swim either by using body and/or caudal fin (BCF) locomotion, by using median and/or paired fin (MPF) locomotion, or by the combination of both BCF and MPF locomotion.

Fig. 1 shows the swimming types identified by the MPF propulsion, based on the extended classification scheme [5,12–13]. Distinction is made based on the fins used and the type of motions performed. The present study focuses on *raj-*

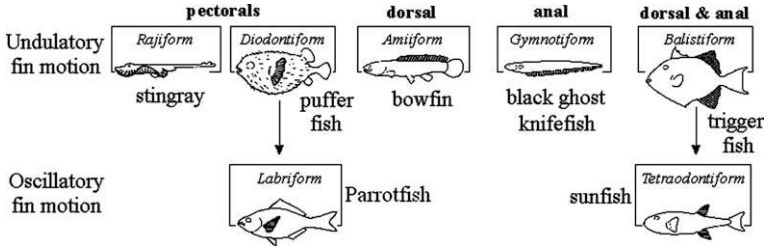

Fig. 1. Sheme of MPF locomotion [5,13].

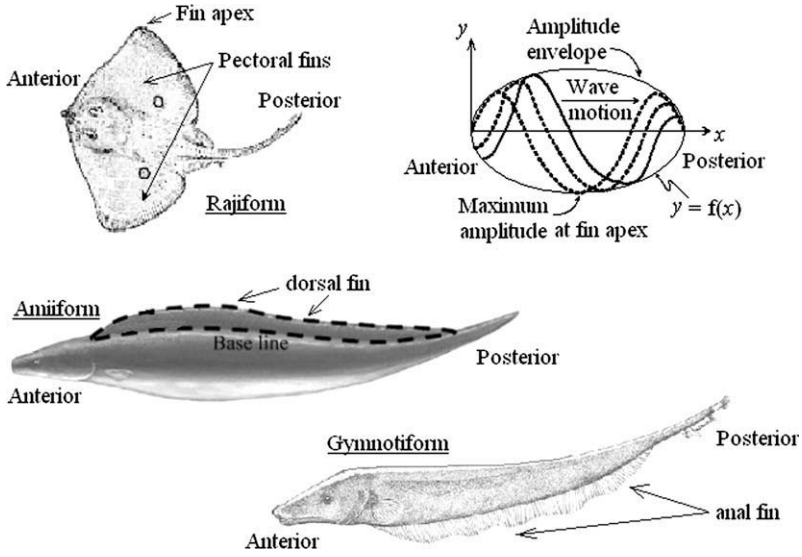

Fig. 2. Morphology of rajiform's stingray (plan view), amiiform's African knifefish (*Gymnarchus niloticus*, side view) and gymnotiform's knifefish (side view) and an estimated amplitude envelope (side view) of the undulating fins associated with their body shapes [16].

iform, *amiiform*, and *gymnotiform* types owing to its long undulating fin locomotion, other types of MPF types can be found in references [14–15].

In *rajiform* type, fin propulsion is generated by passing vertical undulations along the wide pectorals with increasing amplitude from the anterior part to the fin apex and tapers again towards the posterior [13], as shown in Fig. 2. Most of the time, the body of the fish under consideration is held straight when swimming. Typical examples are stingrays, skates and mantas, which are characterized by large, triangular-shaped and flexible pectoral fins (see Fig. 2). Propulsion in *amiiform* is achieved by undulations of a long-based dorsal fin with body held straight, whereas propulsion in *gymnotiform* is by undulations of a long-based anal fin. An example of gymnotiform fish, such as knifefish, does not have dorsal and caudal fins.

2.2. Biomimetic fish robots

Fish and most aquatic animals are efficient swimmers, which have remarkable manoeuvrability, capability to follow desired trajectory, and are able to stabilize themselves in currents and surges. Study and research of these aquatic creatures help us to understand how their biological counterparts are functioning. Biomimetic design of underwater vehicles has therefore attracted the attention of researchers. In general, the biomimetic implementation covers the design of propulsors, buoyancy, and shape of body and fin(s). It is hoped that the fin propulsion vehicles leave a less noticeable wake than conventional underwater vehicles equipped with propeller(s).

Biomimetic fish robots, as a new style of underwater thrusters, can play an important role in many applications. It is a combination of bio-mechanism, engineering technology, and also a multidisciplinary field that involves hydrodynamics based control and actuation technology. In the last decade, some excellent works have developed a robot resembling real

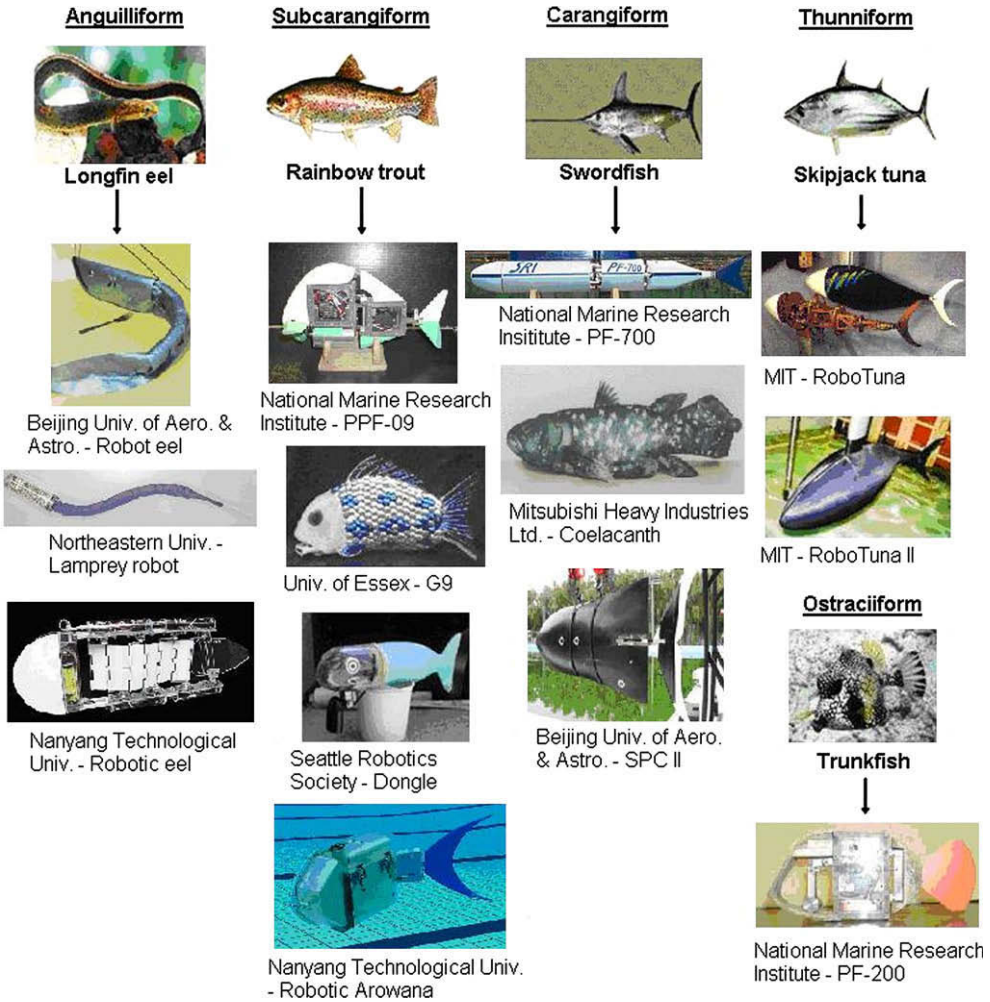

Fig. 3. Examples of BCF fish and the robotic counterpart developed [17–28].

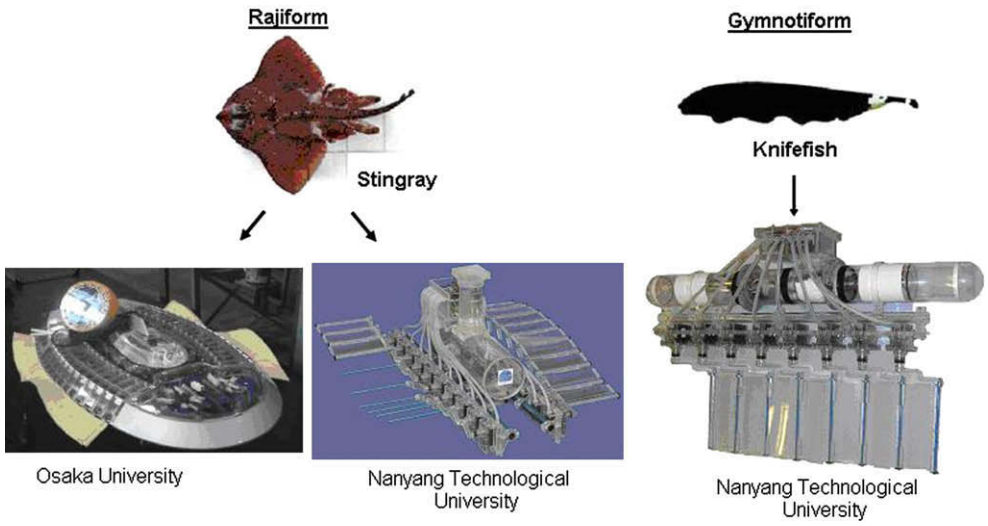

Fig. 4. Examples of MPF fish and the robotic counterpart developed [3,4].

fish. Figs. 3 and 4 illustrate several biomimetic fish developed and tested. These are fish-like aquatic vehicles inspired by the swimming modes and anatomic structure of fish, mainly the undulatory and oscillatory body/fin motions.

2.3. Biological and biomimetic MPF undulation

Undulating swimming modes can be involved in both BCF and MPF locomotion. In BCF types as shown in Fig. 3, the anguilliform like eels involves purely undulating motion. As for the MPF types, the fish generate forward and upward thrust through the undulating/oscillating motion of the long fins (see Fig. 5). Examples can be found in Fig. 4 for the rajiform and gymnotiform prototypes.

Several works [3,4,30–32] have focused on the biomimetics design of undulating fin mechanisms for propulsion means. First of all, a robotic ribbon fin system [30] has been developed and tested [30]. As shown in Fig. 6, the fin mechanism has eight rays connected by a 0.025 mm thick sheet of latex. Each ray is a brass rod, 76.2 mm in length and 1.6 mm in diameter. The distance from the tip of the first ray to the tip of the eighth is 231 mm, when the fin is in its quiescent state.

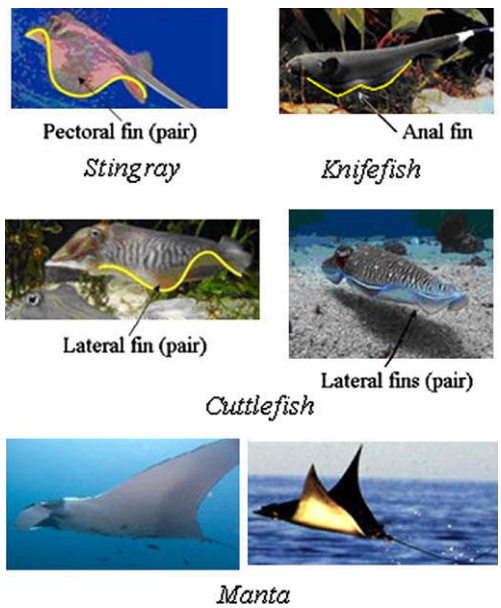

Fig. 5. MPF Fish swimming with long and wide undulating/oscillating fins [28,29].

On the other hand, a team of the Osaka University [3,31] has developed a squid-type underwater vehicle with two undulating side fins, as shown in Fig. 7. The fin model has 17 servomotors for both sides to produce arbitrary fin motion. The model is able to navigate freely in any direction and to change the angle at around any axis. The dorsal fin of the model is to keep

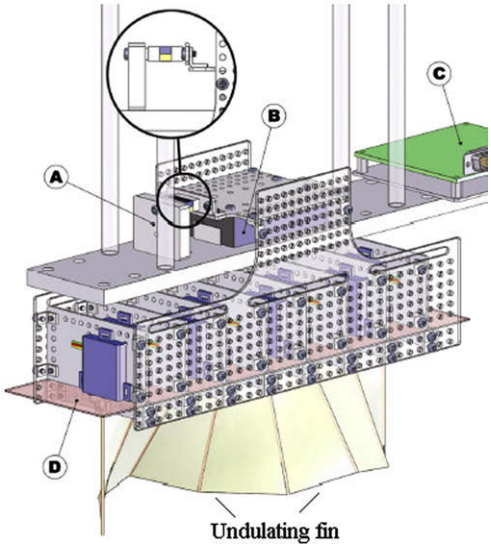

Fig. 6. Robotic ribbon fin developed by the Northwestern University [30].

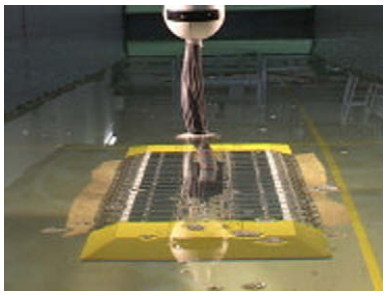

Fig. 7. Squid-type underwater vehicle by the Osaka University [3,31].

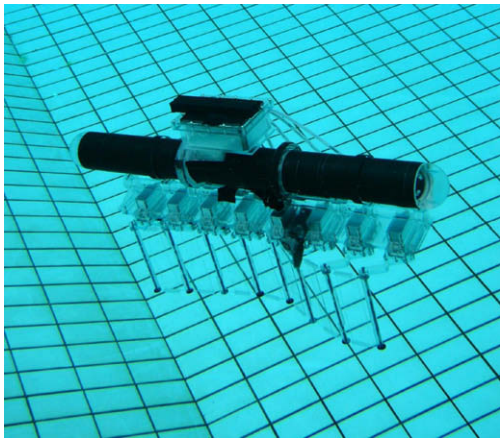

Fig. 8. Nanyang knifefish (NKF-I) robot devloped by the NTU [4].

a desired direction, while its caudal fin is to change the depth. For control purposes, a thin cable is connected to the floating wireless communication units and to the computer as well.

In another prototype development, Low and Willy [4,19,32] of the Nanyang Technological University (NTU) have designed and constructed a knifefish robot with modular fin mechanisms (NKF-I). As shown in Fig. 8, the fin segment is able to fully produce undulation motion by virtue of the designed crank-slider linkages (further discussion in the next section).

3. Modeling of fin mechanisms

3.1. Mechanism design of fin rays

The fin propulsion plays an important role in design of fish robots. In a recent work [4,19,32], biomimetic fin propulsion has been achieved by making use of modular fin mechanisms together with *sliders* (see Fig. 9). The complete fin mechanism is able to provide various waveform shapes. As shown in Fig. 9a, the fin consists of specified number of servomotors. Each of them drives a crank that is connected to the slider. For example, six sliders will be required for seven cranks. The sliders can retract and extend on their own within an allowable length, as illustrated in Fig. 9b. The kinematics diagram of the five-bar mechanism is shown in Fig. 9c. It is seen that link 3, link 4 and the slider *C* are always formed in a straight line with adjustable link length ef (points e to f). The assembled fin ray for arbitrary waveform is shown in Fig. 9d.

As introduced in the previous section, Epstein et al. [30] and Toda et al. [31] use a cam-driven mechanism to produce the up-and-down oscillation motion of fin rays. The rotational axis of their models is *parallel* to the longitudinal wave direction. The fin-ray configuration is different from the model by the crank-slider four-bar fin mechanism developed by Low and Willy [4,32], in which the rotational axis is *perpendicular* to the longitudinal wave direction. The single crank rotation of the ray is similar to the pedals of a bicycle. Note that the fin motion by virtue of the crank-slider can be both oscillating and undulating. With the slider, the amplitude of the fin motion can be varied. It is also worth mentioning that, by virtue of modular and scalable design, various types of biomimetic can be modeled by different number and arrangement of the undulating fin(s), as depicted in Fig. 10.

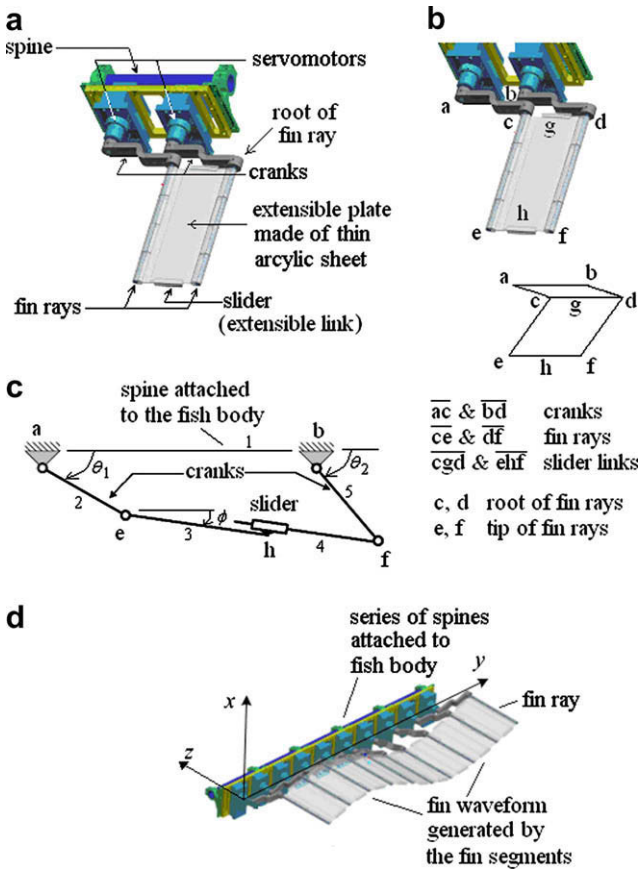

Fig. 9. Modular fin mechanism: (a) single segment with two motors; (b) relation of cranks, servomotors, and rays; (c) kinematics diagram of the single five-bar mechanism with a slider; (d) assembly of fin segments [4].

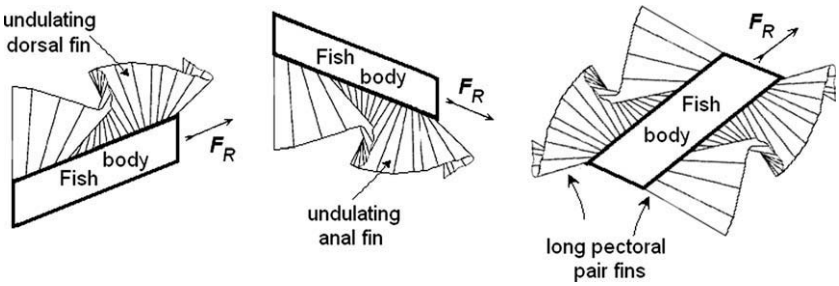

Fig. 10. Fin undulations found in amiiform, gymnotiform, or rajiform.

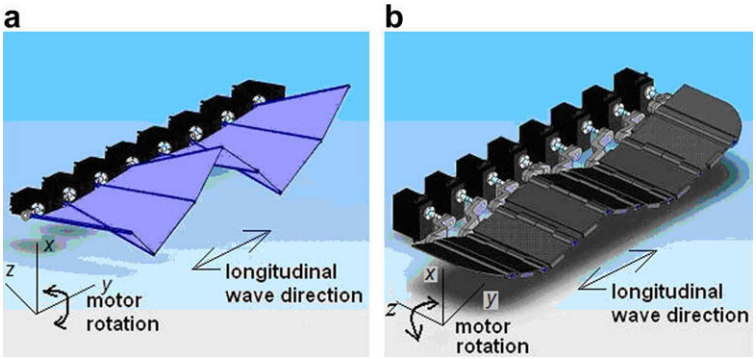

Fig. 11. Fin-ray segments driven by (a) cam mechanism [30,31]; (b) crank-slider linkage [4,19].

As for another comparison, it is seen that in Epstein [30] and Toda's [31] models, the base longitudinal axis of the fin segments and the tip longitudinal axis of the fin segments can be formed in an inclining straight line, depending of the rotation angle. On the other hand, the base longitudinal axis of the fin segments in Low and Willy's model [4] is moving in the same horizontal plane of the tip's longitudinal axis of the fin segments, as shown in Fig. 11. In fact, we should find out in future study, which of the undulating in Figs. 11a and 11b is more energy efficient.

3.2. Kinematics modelling of fin rays

Undulating fins with a fixed baseline, such as those developed by the teams of Toda [3], Hu [11], and Epstein [30], have been unified in a ruled-surface-based kinematics model. Their undulating fin can be modeled as a ruled surface in 3-D space. The fin baseline is the directrix of the ruled surface, while the fin ray is the generatrix, as shown in Fig. 12. The undulation can then be generated through a sequential oscillating of generatrix on the ruled surface. Here, the undulating fin wave can be modeled by the ruled-surface expression [11]

$$\boldsymbol{p}(r,s,t) = \boldsymbol{b}(s,t) + rd(s)\boldsymbol{c}(s,t), \quad 0 \le r \le 1 \tag{1}$$

where $\boldsymbol{b}(s,t)$ is the fin base curve that describes the change of the respective fin ray's starting point along the fin base, $\boldsymbol{c}(s,t)$ is a time-varying vector overlapping the fin ray at $y = s$, $d(s)$ is the length of the fin ray at $y = s$, t is the time, and r is a normalized

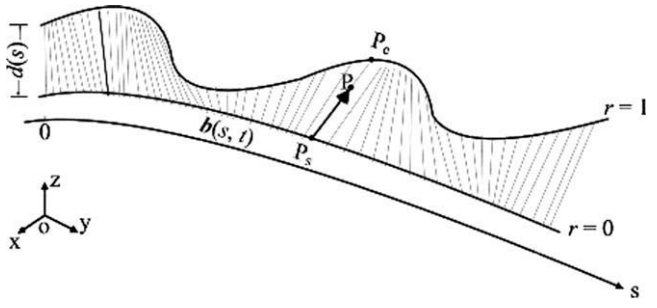

Fig. 12. Ruled-surface-based kinematical model for the undulating fin with fixed base at $r = 0$.

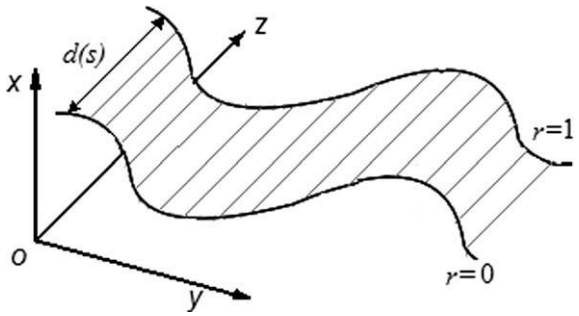

Fig. 13. Model of the undulating fin with free base (along $r = 0$).

non-dimensional parameter defining the ratio of $|P_sP|$ to $|P_sP_e|$. Note that $|P_sP|$ is the length from any point on the surface to its corresponding start, and $|P_sP_e|$ denotes the length of the fin ray on which the point is located.

The modelling of the fin by Low and Willy [4] can be simplified due to its free base line design (see Fig. 9d and Fig. 13). The generatrixes on the ruled surface are kept parallel when cranks oscillate. The motion function by Lighthill [33] is used to model the undulating fin:

$$x(y,t) = (c_1 y + c_2 y^2)\sin(2\pi\alpha\ t + ky) \tag{2}$$

where x is the amplitude of the undulating wave, y-axis is the centre line of the wave, c_1 is the linear wave amplitude envelope, c_2 is the quadratic wave amplitude envelope, α is the wave frequency, and $k = 2\pi/\lambda$ is the wave number associated to the wavelength λ. The motion Equation, Eq. (2), has widely been used in the locomotion of fish robots.

In order to model the multi-degree-of-freedom propulsor, we rewrite Eq. (2) as

$$x(y,t) = (c_0 + c_1 y + c_2 y^2)\sin(2\pi\alpha\ t + ky) = C\sin(2\pi\alpha\ t + ky) \tag{3}$$

where c_0 is the profile of undulating fin at the initial or starting point. The envelope parameters c_1 and c_2 can be obtained by the behaviours observation of real fish. By virtue of c_0 in Eq. (3), we assume that the amplitude x at $y = 0$ can be any value, which is required in a general prototype design. To enhance the performance of the fish robot, we can also utilize the CFD tools or experiments to find the optimal values of these parameters. Note that the fin undulating will form a harmonic wave, if the envelop modulating term C of Eq. (3), $c_0 + c_1 y + c_2 y^2$, is a constant. The simplified wave control method of fins (with the constant amplitude C) will be considered in the following discussion.

3.3. Undulating fin rays with sliders

Fig. 14 depicts the basic waveform of the fin segments connecting in series. The waveform in isometric view can be found in Fig. 9d. The crank's root point at the horizontal line shows the position of each respective servomotor. The lines away from the root points represent the respective cranks (for example, ac and de in Fig. 9b). The lines connecting the tip points of the cranks form the resulting fin wave, which is pushing away the water to provide the locomotion.

As shown in Fig. 14, the membrane between two fin rays is a straight line joining the tip point of the two adjacent cranks. A set of straight lines joining these points, line abcdefgh, represents discrete lines to form an approximate sinusoidal wave with adjustable amplitudes. The mechanism is able to provide an equivalent flexible length by virtue of the respective slider (for example, changing length ab).

The modular concept enables us to easily and conveniently construct various biomimetic fish robots swimming by fin undulations in different forms, while the re-configurable assembly allows us to construct the fish robots in different forms

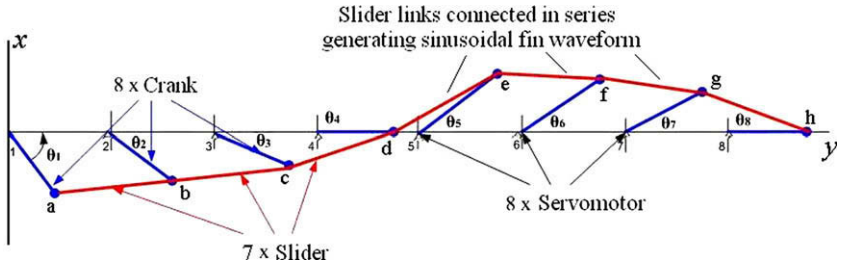

Fig. 14. Discrete model of sinusoidal waveforms developed by series of straight lines joining two points in various phase angles and undulating fin connecting all cranks. Seven servomotors are assumed in the figure. The parameter $c_0 = 0$ for the configuration shown and the axis $y = s$.

by changing the number of fin rays [34]. With these features, we are also able to attach single or multiple sets of fin spines to any position of the fish body, as shown in Fig. 10.

3.4. Waveform of fin rays generated by inter-connected slider links

We can now model a propulsive wave as a basic sinusoidal function, formed by the roots of the fin rays oscillating at the same frequency but out of phase, as shown in Fig. 14 (or Fig. 11b in isometric view).

To investigate the waveform generated by a series of crank-slider five-bar mechanisms, it is useful to define the geometry of single fin pairs. As depicted in Fig. 15, R is the crank length, L the distance between two servomotors, S the length of the slider, $S_{\min}$ the minimum possible length of the slider (when slides are fully retracted), $S_{\max}$ the maximum possible length of the slider (when sliders are fully extended), θ_1 the angular position of a crank attached to the 1st servomotor, and θ_2 the angular position of a crank attached to the 2nd servomotor.

The multi-actuation fins together with the sliders can accommodate various amplitude envelopes and wavelengths. In other words, we are able to model and generate a fin profile, with arbitrary amplitudes along the fin, at each individual segment by controlling the actuator angles, θ_n. This will in turn allow us to provide an arbitrary and predictable fin wave [34].

Fig. 16 illustrates the basic layout of the waveform with respect to the fin geometry. The joint variables θ_n shown in the figure are related to the wave amplitude, crank length and phase angle γ_n ($n = 1, 2, \ldots, m$). For example, we can write θ_2 as

$$\sin\theta_2 = \left(\frac{x_2}{R}\right) \tag{4}$$

and

$$x_2 = A_2 \sin\gamma_2 \tag{5}$$

The substitution of Eqs. (5) into (4) yields

$$\theta_2 = \sin^{-1}\left(\frac{A_2 \sin\gamma_2}{R}\right) \tag{6}$$

in which the phase angle γ_2 is the only variable.

Since γ_n rotates reciprocately, we can assume that it subjects to the following function:

$$\sin\gamma_n(t) = \sin[2\pi\alpha t + (n-1)\beta] \tag{7}$$

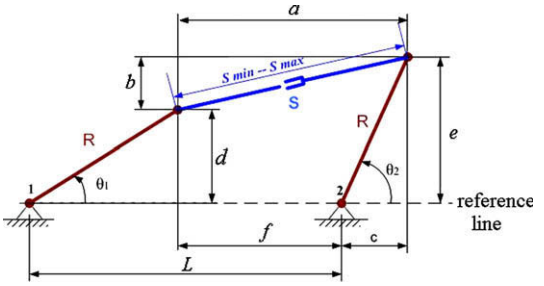

Fig. 15. Geometry for the calculation of slider length, S, in a single fin segment.

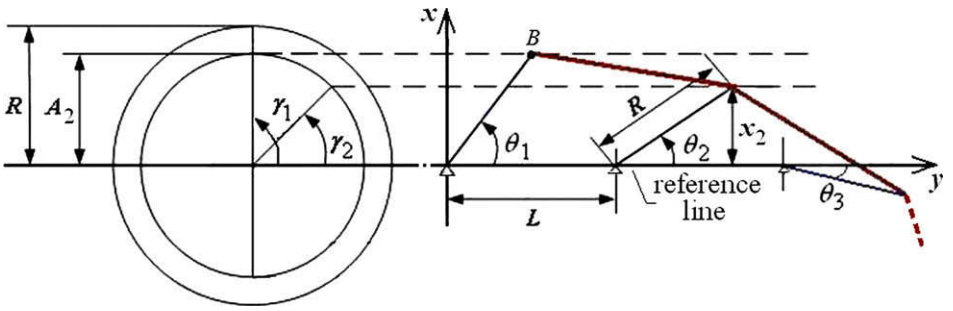

Fig. 16. Basic layout for the waveform, in which A is the amplitude of a resulting sinusoidal movement, x is the vertical height from the crank end to the reference line, θ_i is the angular position of a crank attached to the ith servomotor, where $i = 1, 2, \ldots, m$, where m is the total number of motors (only the angle of the three motors, θ_1, θ_2, θ_3, are shown in the figure).

where n is the servomotor number along the longitudinal axis, α is the fin undulating frequency, and $\beta = \gamma_n - \gamma_{n-1}$ is the phase difference (difference of the two adjacent phase angles), which is assumed to be constant in the present study.

By virtue of Eq. (7), the general expression for the angular position $\theta_n(t)$ of a crank attached to nth servos at time t can be written in *nonlinear* form as

$$\theta_n(t) = \sin^{-1}\left(\frac{A_n \sin\gamma_n}{R}\right) = \sin^{-1}\left\{\frac{A_n \sin[2\pi\alpha t + (n-1)\beta]}{R}\right\} \tag{8}$$

where A_n is the amplitude of the nth undulating fin crank.

3.5. Discussion on displacement expressions

By now, we should be able to use different kinematics expressions to generate a sinusoidal waveform of fin segments. First of all, we can use Eq. (8) as the joint control law to drive servomotors. By specifying amplitude A_n, phase difference β, and the frequency α, the motion of each respective motor and the motion of undulating fins can be determined.

The governing equation for the servomotor joint motion control can be simplified further. Our aim is to use the fin segment to generate a sinusoidal wave, say, a harmonic wave. The transmission of such a wave can be thought of vibrations of infinite successive particles. By using the parameters shown in Fig. 16, the wave equation by x can be interpreted as

$$x = A\sin\left(2\pi\alpha t + \frac{2\pi}{\lambda}y\right), \quad 0 \leqslant y \leqslant (n-1)L \tag{9}$$

where λ is the wavelength of the whole undulating fin.

In the undulating fin mechanism shown in Fig. 16, the distal end point of crank, B, acts as the oscillating particle to generate the harmonic wave described by Eq. (9). The independent variable y will then be discretized as

$$y = (n-1)L, \text{ where } \quad n = 1, 2, \ldots, m \tag{10}$$

By substituting Eqs. (10) into (9), we obtain the wave equation in discrete form associated to the distal end of individual cranks as

$$x_n = A\sin\left[2\pi\alpha t + \frac{2\pi}{\lambda}(n-1)L\right] \tag{11}$$

If the crank rotates at a constant speed, the projection of point B on the x axis satisfies a harmonic vibration equation, which provides a harmonic wave along the undulating fin segments. In this case, the control law for a single motor in one vibration cycle can be simply expressed by the *linear* equations as

$$\theta_n(t) = \begin{cases} \theta_{\max}(4\alpha t) & t \in [0, \frac{1}{4\alpha}) \\ \theta_{\max}(2 - 4\alpha t) & t \in [\frac{1}{4\alpha}, \frac{3}{4\alpha}) \\ \theta_{\max}(-4 + 4\alpha t) & t \in [\frac{3}{4\alpha}, \frac{1}{\alpha}) \end{cases} \tag{12}$$

where

$$\theta_{\max} = \sin^{-1}\frac{A}{R} \tag{13}$$

in which $\theta_{\max}$ is the extreme position of crank, which is determined by the waveform amplitude A given in Eq. (13).

We have so far presented two different joint control laws given by Eqs. (8) and (12), respectively. If the control law given by Eq. (8) is applied, every distal end point of cranks perfectly fits a sinusoidal wave at a specified time. However, as the time

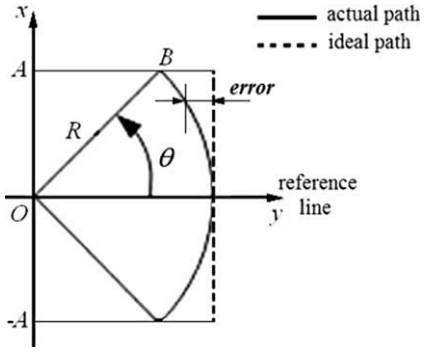

Fig. 17. Error due to the approximated displacement expression.

changes, these points fit different sinusoidal waves. As for Eq. (12), we try to fit the same harmonic waveform for all distal ends at any time instant.

It should be noted that the fin wave defined by Eqs. (8) or (12) is merely an approximated sinusoidal wave. On one hand, the connecting segment between two cranks is a straight and rigid link, which is unable to resemble a sinusoidal curve. On the other hand, the actual path of distal point of crank is a circular arc, which is not exactly the same as the desired vertical path (dash line) shown in Fig. 17. Both scenarios introduce errors. As the range of the phase angle is limited by workspace (which will be discussed in the next section), the error depicted in Fig. 17 is small and is therefore negligible.

In our prototype, the control law specified by Eq. (12) is adopted and can be easily implemented on hardware owing to the linear equation(s). The cost of control implementation will then be reduced greatly, especially when many servomotors are used in one fish robot.

4. Parametric study of fin motion

4.1. Limits of workspace

Fig. 18 displays the slider's workspace generated by the motion of two cranks with the parameters defined in Fig. 15. Note that all crank angles in series are in the range of $-90°$ to $90°$, owing to the geometry constraint [34]. For further explanation, three designated positions have been marked in Fig. 18. As shown in Fig. 19, the three positions represent one working area and two limits of slider's positions: (a) slider moves smoothly within the working area, position P_1, (b) slider reaches the end of the track when it hits the blue lines, position P_2 (left-right boundaries), and (c) slider gets disconnected when hitting the red lines (up-down boundaries), position P_3.

At a given undulating frequency of fin, it is assumed that larger amplitude of the fin motion provides higher thrust force. In actual prototype design, the maximum amplitude of actual fin motion depends on several factors, such as the allowable length of slider S, the length of the crank R, the ranges of rotation angle of crank θ, and the distance between the roots of cranks L.

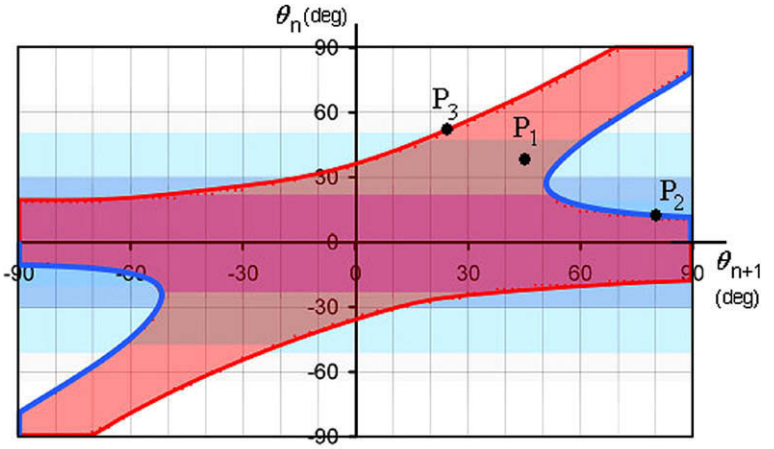

Fig. 18. Workspace of the slider on the connecting link between two cranks (limits: slider hits end of track; slider disconnects). (For interpretation of the references to colour in this figure legend, the reader is referred to the web version of this article.).

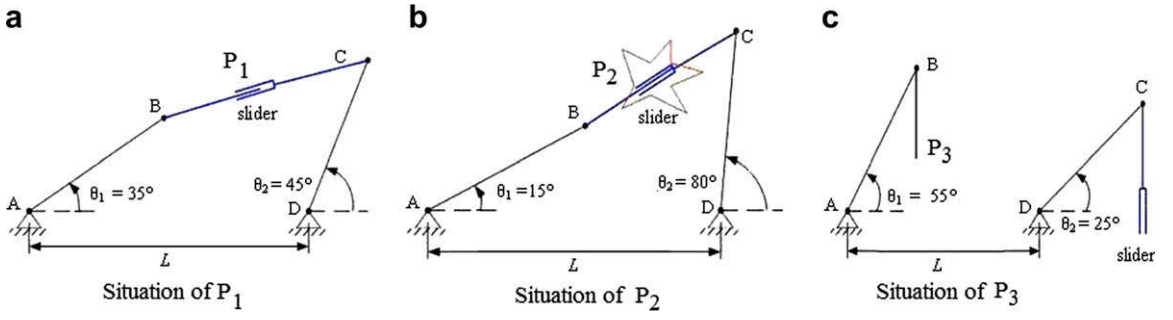

Fig. 19. Sliders move within the working area at P_1; hit the end of track at P_2; and get disconnected at P_3.

4.2. Effect of phase difference and amplitude on fin waveforms

In this section, we would like to present the parametric study of the undulating wave for the complete fin segments shown in Fig. 14. First of all, it is useful to find out which phase difference is suitable to generate fin sinusoidal motion.

Fig. 20 illustrates the workspace and the wave profiles of the fin segments in terms of various phase differences β, by using Eq. (8). Note that the results in Fig. 20 are obtained based on the constant parameters (see Fig. 16): $L = 70$ mm, $R = 60$ mm, and $A = 41$ mm. It was found that, for a suitable fin design, the phase difference β should be between 30° and 90° to generate a sinusoidal locomotion.

Let us now investigate the effect of crank amplitudes on the fin waveforms. The results will be presented respectively for constant, increasing and decreasing consecutive amplitudes of the cranks, $A_1, A_2, \ldots, A_n$. As illustrated in Fig. 20, as the fin segments oscillating and undulating with constant amplitude, the associated amplitude envelope will define the oscillation path of the cranks of the servomotors, which can then be mapped into one circular path. Fig. 21 demonstrates that different amplitude trends of the crank series will generate different sinusoidal waveforms. As we can see from Fig. 22, the changing in amplitude (with the same phase difference) will have a significant effect on the waveform, i.e. larger amplitude will lead to bigger waveform, and vice versa. Of course, the maximum allowable amplitude will depend on the allowable workspace (to be discussed in Section 4.3).

4.3. Comparison and discussion of workspaces

Given R and L in a single fin segment (see Fig. 5), the allowable range of slider's length will determine the workspace of fin mechanisms. We shall now find a suitable geometry of S for the fin design, and to deduct possible largest amplitudes of the sinusoidal motion. Note that the parameter study is concerned with the fin design to provide an arbitrary sinusoidal movement with amplitudes as larger as possible.

As shown in Fig. 15, the length of slider S between two cranks is changeable by the combination of two independent joint angles. The length of the slider S can be derived as follows:

$$S = \sqrt{a^2 + b^2} \tag{14}$$

in which

$$a = c + f = R\cos\theta_2 + (L - R\cos\theta_1) \tag{15}$$

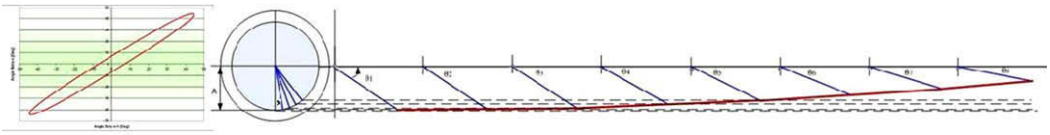

(a) Motion with phase difference, $\beta = 10^\circ$. Not a sinusoidal movement of fin locomotion.

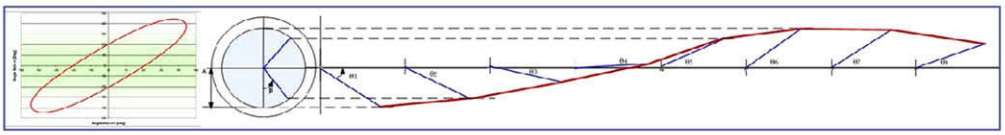

(b) Motion with phase difference, $\beta = 30^\circ$. Producing a sine wave of 180°, suitable for fin locomotion.

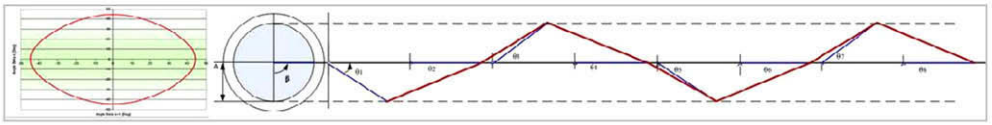

(c) Motion with phase difference, $\beta = 90^\circ$. Producing one and a half unsmooth sine wave.

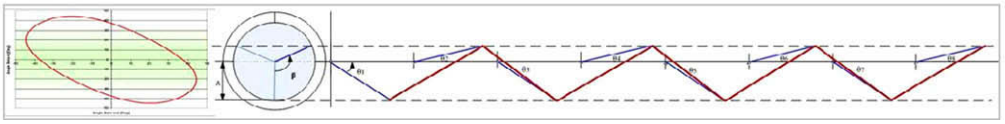

(d) Motion with phase difference, $\beta = 120^\circ$. The wave produced is not a sinusoidal movement.

Fig. 20. Workspace and waveform of the respective fin segments with different phase differences β (given the same length L and the number of motors).

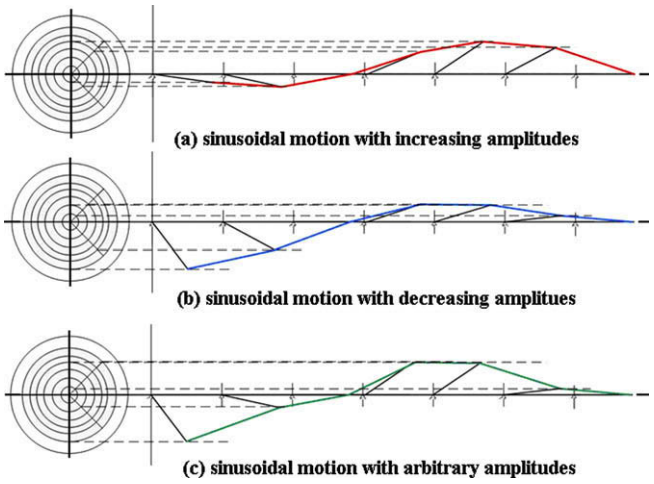

Fig. 21. Various fin sinusoidal waves generated.

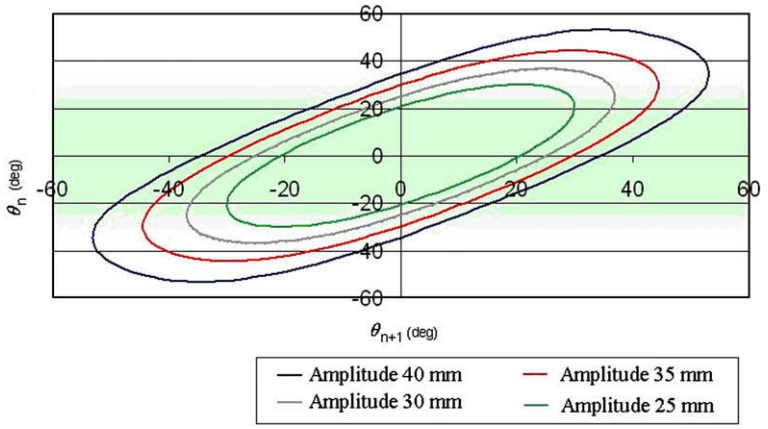

Fig. 22. Waveforms with different amplitudes ($\beta = 30°$).

$$b = e - d = R\sin\theta_2 - R\sin\theta_1 = R(\sin\theta_2 - \sin\theta_1) \tag{16}$$

Therefore, the length of the slider is given by

$$S = \sqrt{(R\cos\theta_2 + L - R\cos\theta_1)^2 + (R\sin\theta_2 - R\sin\theta_1)^2} \tag{17}$$

which is written in terms of the two crank angles. Again, the range of the angles θ_1 and θ_2 is between $-90°$ and $90°$.

The objective of the parametric study is to find possible maximum amplitude with the phase range of 30°–90° at any given geometry of slider. It is found that a larger crank angle will produce higher amplitude. The increase of the crank angle will however decrease the allowable phase difference, which will then constrain the performance of the whole fin. Therefore, we need to devise a method to balance both of them.

To this end, an area ratio is introduced to compare different workspaces for a comprehensible solution. As illustrated in Fig. 23, the area ratio is defined as

$$\eta(\%) = \frac{P^2}{Q^2} \times 100 \tag{18}$$

where Q is a constant ($Q = 180°$) and P ($P = \min\{P1, P2\}$) is the smaller length to determine the working square area (P^2).

With the defined area ratio η, we will find out a set of parameters of the single fin segment by investigating different workspaces. The ratio implies how much usable area of the workspace, by virtue of the workspace limits set in Fig. 18. Note that the workspace is associated to two adjacent joint angles. Accordingly, the maximum ranges of workspace can be obtained for a given fin waveform in terms of the joint angles. In the following computation, the crank length and the distance

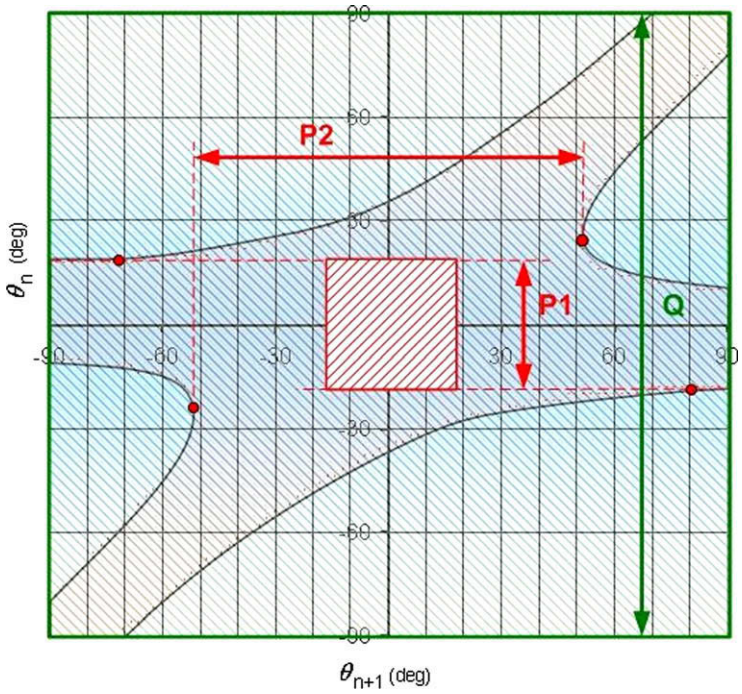

Fig. 23. Workspace with the defined area ratio.

between servomotors are selected as $R = 60$ mm and $L = 70$ mm, which is a suitable selection for the actual mechanical design. The values of S_{min} and S_{max} are then varied to find a desired workspace. Some results obtained are listed in Table 1, in which Workspace 4 gives the highest area ratios, among many workspaces that computed. It should be noted that the result can only be an approximated guide, as the area ratio is defined by a square, instead of the actual work area formed by curves.

As a result of the motion studies (details not shown here for clarity), a fin mechanism design providing good workspaces has been obtained. The fin segment is expected to achieve a maximum amplitude of about 42 mm. Fig. 24 shows the resulted workspace of the selected fin dimension (see Workspace 4 in Table 1) with five different phase differences (30°–90°).

5. Sample fish robot with undulating fin segments

As shown in Fig. 25a, an improved prototype of assembled knifefish robot (NKF-II) has been developed and tested. The NKF-II is black in colour resembles knifefish. Also, the fin dimensions obtained in the parametric study, $L = 70$ mm and $R = 60$ mm in Fig. 15, has been used for all cranks, as shown in Fig. 25b.

The fish robot comprises of three individual modules: buoyancy tank module, motor compartment module, and undulating fin module [34]. As they are designed in a modular manner, these modules can be easily replaced should there be a change in the design or additional functions are required to be attached to the NKF-II.

The control for the buoyancy tank required one BasicX-24p microprocessors while the undulating fins required another BasicX-24p microprocessors and one servomotor controller – servo 8 T. The power source for the two systems consists of two separate 7.2 V 3A-batteries in order to prevent problems in the transmission of data and signals between the microprocessors. Table 2 shows the main specifications of the NKF-II. The undulating fin module is made up of seven fin segments, which mimic the swimming gaits of the black ghost knifefish, as shown in Fig. 26.

Table 1
Results of the area ratio for workspaces with different values of S_{min} and S_{max} ($L = 70$ mm and $R = 60$ mm).

Workspace no.	S_{min} (mm)	S_{max} (mm)	P (deg)	η (%)	A (mm)
1	57	104	76	18	36.9
2	58	106	80	20	38.6
3	59	108	83	21	39.7
4	60	110	88	**24**	**41.7**
5	61	112	84	22	40.1

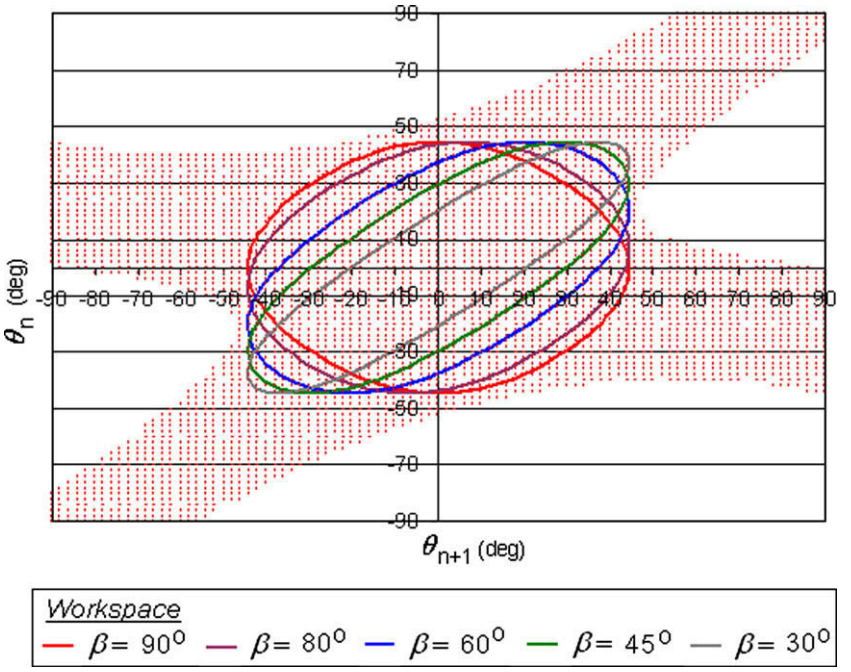

Fig. 24. Allowable fin workspace in terms of adjacent phase differences β.

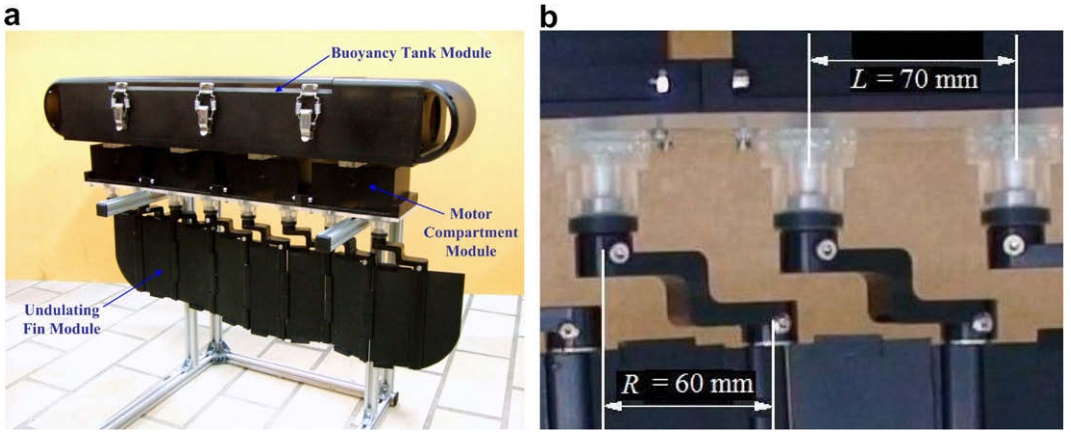

Fig. 25. Fully assembled Nanyang knifefish II (NKF-II) (a) Integration by three modules; (b) detailed view of crank's dimension.

Table 2
Main specifications of NKF-II.

Biomimetic Nanyang knifefish (NKF, version 2) robot	
Mass	11.62 kg
Color	Black
Material	Mostly acrylic and delrin
Length	70 cm
Height	42 cm
Width	13.5 cm
Micro-controller	BasicX-24p microprocessor
Actuator	Futaba S3801 servomotor (8 units), Futaba S5801 servomotor (2 units)
Undulating fin segments	Total of seven segments (L = 70 mm, ray to ray in a single segment)
Buoyancy force	113.44 N ($F_B = \rho_f g V_f$)
Gravity force	114 N ($F_G = \rho_b g V_b$)
Buoyancy	−0.5 N (slightly negative buoyancy with motors and battery)

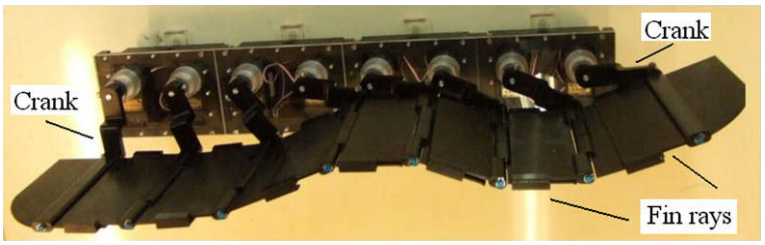

Fig. 26. Sinusoidal waveform created by the undulating fin of NKF-II (bottom view).

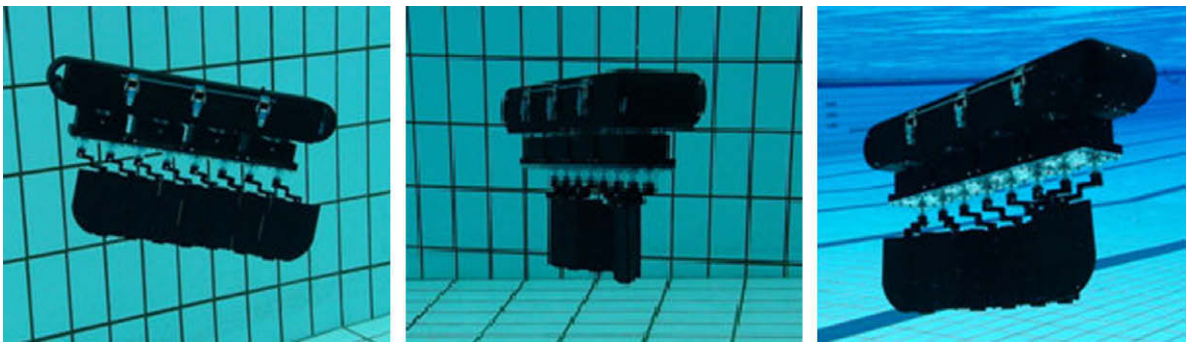

Fig. 27. Snapshots of NKF-II taken in the NTU swimming pool.

Initial experiments and testing of the designed NKF-II have been conducted in the NTU swimming pool. The knifefish robot was also deployed in the 4-meter depth diving pool to simulate the actual operating condition with deep water pressure and the water current resulted from the filtration system in the diving pool and the surface wind. Fig. 27 depicts three snapshots of the NKF-II tested under water. Note that the fish robot was operated by using a radio frequency remote controller.

6. Concluding remarks

This paper has presented biomimetic design and fin workspace study of fish robots with the undulating fins mechanisms. The fish considered are in those with long and/or wide undulating fin, especially those of anguilliform, amiiform, rajiform, and gymnotiform. Two fin-ray mechanism layouts to produce arbitrary undulating fin waveform have been discussed and compared. Among them, the fin mechanism with the slider connecting in series is able to generate arbitrary undulating waveforms. The kinematics expression of the associated waveform is derived. A parametric study on the fin workspace enables us to develop a series of fin rays by making use of the crank dimension obtained. The equations of slider's displacement and fin waveform are firstly discussed. Given the amplitude and the phase difference, the associated workspace and wave profile of fin segments are studied. Working range and limitations of the slider in relation to the workspace of fin segments are also illustrated.

A fish robot is then formed by integrating a buoyancy tank to the fin mechanisms. Owing to the modular and configurable features, the designed fish robot and the fin mechanisms can easily be modified to model fish robots with different fin attachments and layouts. On the other hand, the battery, actuation, and control units are placed inside the buoyancy tank for ease of waterproofing, assembling, and maintenance [35]. Initial pool testing has been conducted to demonstrate the swimming locomotion and the performance of the fish robot.

More tests and investigations should be conducted to understand the impact of design parameters to the robot's performance and efficiency. Improved design of the existing prototype should also be explored for compactness, easier waterproofing, energy-saving fin motion, etc. Passive or elastic components could be a way to optimize the energy [36–37]. Future study should investigate which of the undulating layouts depicted in Figs. 10a and 10b is more energy efficient. In addition, hydrodynamics should be incorporated in future work for efficient swimming and a better controlling of the fish robot in response to external disturbances. Useful body/fin materials, effective payload capability, communication, and team coordination of the fish robot are some other worth-exploring research areas. It is interesting to note that that the real fish follow simple rules that keep the group alert and be communicated: stick together, avoid collisions, and swim in the same direction [38]. The future study of swarm intelligence can then provide us much insight in designing biomimetic underwater robots for complex group coordination tasks. On the other hand, the application of flexible fin materials is an area worth exploring. The flexible beam or plate formulation [39–41] is therefore required for the modelling of fin segments and body structures.

As for the actuation, the hybrid driving system with smart materials [42–44] and servomotors will be a useful design methodology for future fish robots.

Although the biologists have done excellent jobs in providing us details on the fish swimming gaits and their functioning features, the engineers and roboticists should not expect a wonderful biomimetic performance, at least over this decade, in view of the current limitation of actuators, sensors, and communication technology required for underwater tasks. How much we can learn and we should apply from nature remains an interesting and challenging research works ahead for us.

It is also important for us to understand the distinction between biological *mimicry* (or biomimetics) and biological *inspiration*. A completely or exact biomimetic fin undulation solution is difficulty to design with current technology and may be even more difficult to implement. On the other hand, biological inspiration may lead to a better solution for a given space than that afforded by the biological entity itself. Therefore, any biological model should serve as a good starting point, but the design must not be constrained by the limitation of the model – in fact, going beyond the biological model could provide an even better solution than the original source of inspiration.

Acknowledgements

The author would like to thank the reviewers for their constructive comments, which have greatly improved the quality of the paper. Thanks are also due to Chunlin Zhou and Tianjiang Hu for their help in the proof-reading of the paper, Miss Hui-Fong Poea for her good work in the development of NKF-II, and Chee-Wee Chong for his help in paper preparation. Thanks are also due to the students, Andre Willy, Wai-Leong Aw, and Christian Eigenmann for their assistances in the development of relevant prototypes helpful to the present work. Facility support and technicians assistance at the Robotics Research Centre, NTU, is also appreciated.

References

[1] V. Lauder, E.G. Drucker, Morphology and experimental hydrodynamics of fish fin control surfaces, IEEE Journal of Oceanic Engineering 29 (3) (2004) 556–571.
[2] J. Edward Colgate, Kevin M. Lynch, Mechanics and control of swimming: a review, IEEE Journal of Oceanic Engineering 29 (3) (2004) 660–673.
[3] Y. Toda, T. Suzuki, S. Uto, N. Tanaka, Fundamental study of a fishlike body with two undulating side-fins, Bio-Mechanisms of Swimming and Flying (2004) 93–110.
[4] A. Willy, K.H. Low, Development and initial experiment of modular undulating fin for untethered biorobotic AUVs, in: Proceedings of the International IEEE Conference on Robotics and Biomimetics (ROBIO05), Hong Kong, 2005, pp. 45–50.
[5] M.S. Sfakiotakis, D.M. Lane, J.B.C. Davies, Review of fish swimming modes for aquatic locomotion, IEEE Journal of Oceanic Engineering 24 (2) (1999) 237–252.
[6] G.V. Lauder, Peter G.A. Madden, Learning from fish: kinematics and experimental hydrodynamics for roboticists, International Journal of Automation and Computing 3 (4) (2006) 325–335.
[7] B. Kim, D.-H. Kim, J. Jung, J.-O. Park, A biomimetic undulatory tadpole robot using ionic polymer-metal composite actuators, Smart Materials and Structures 14 (2005) 1579–1585.
[8] J.W. Paquette, K.J. Kim, Ionomeric electroactive polymer artificial muscle for naval applications, IEEE Journal of Oceanic Engineering 29 (2004) 729–737.
[9] S. Guo, T. Fukuda, K. Asaka, A new type of fish-like underwater microrobot, IEEE/ASME Transactions on Mechatronics 8 (1) (2003) 136–141.
[10] How ships' traffic noise affects whales in a shipping channel. <http://www.pbs.org/odyssey/odyssey/20030506_log_transcript.html> (accessed May 2006).
[11] Tianjiang Hu, Lincheng Shen, Fei Li, Guangming Wang, Xiaoyun Han, Kinematic modelling and the motion algorithm for the long undulatory fin, Control Theory and Applications 26 (1) (2009) 1–7 (in Chinese).
[12] C.M. Breder Jr., The locomotion of fishes, Zoologica 4 (1926) 159–291.
[13] C.C. Lindsey, Form function locomotory habits in fish, in: W.S. Hoar, D.J. Randall (Eds.), Fish Physiology VII Locomotion, Academic, New York, 1978, pp. 1–100.
[14] R.W. Blake, On balistiform locomotion, Journal of the Marine Biological Association of the United Kingdom 58 (1978) 73–80.
[15] R.W. Blake, The mechanics of labriform locomotion. II. An analysis of the recovery stroke and the overall fin-beat cycle propulsive efficiency in the angelfish, Journal of Experimental Biology 85 (1980) 337–342.
[16] A. Willy, Design and Development of Undulating Fin, Master Thesis, School of Mechanical and Aerospace Engineering, Nanyang Technological University, Singapore, 2005.
[17] X. Dai, Some New Progress of Advanced Robotics in China. <http://www.iai.csic.es/iarp/sapr/05_CHINA_IARP_JCF_2003.pdf>, 2003 (accessed October 2007).
[18] Joseph Ayers et al., Biomimetic Underwater Robot Program in Marine Science Center, Northeastern University. <http://www.neurotechnology.neu.edu/> (accessed October 2007).
[19] K.H. Low, Gerald G.L. Seet, C. Zhou, Biomimetic design and workspace Study of a compact and modular undulating fin body segments, in: Proceedings of the 2007 IEEE International Conference on Mechatronics and Automation (ICMA07), Heilongjiang, China, 2007, pp. 129–134.
[20] National Maritime Research Institute, Model Fish Robot: PPF-09. <http://www.nmri.go.jp/eng/khirata/fish/model/ppf09/index_e.html>, 2002 (accessed October 2007). <http://www.nmri.go.jp/eng/khirata/fish/model/modele.htm>.
[21] University of Essex, G9 Robotic Fish. <http://privatewww.essex.ac.uk/~jliua/picgallery.htm#G9>, 2006 (accessed October 2007).
[22] D. Massie, et al., Autonomous Robotic Fish, Dongle, Seattle Robotics Society. <http://www.seattlerobotics.org/encoder/200211/autonomous_robotic_fish.html> (accessed October 2007).
[23] K. Hirata, Prototype Fish Robot, PF-700, National Maritime Research Institute. <http://www.nmri.go.jp/eng/khirata/fish/experiment/pf700/pf700e.htm>, 2001 (accessed October 2007).
[24] Mitsubishi Heavy Industries, Ltd. 70 cm Long "Coelacanth" to be displayed at Aquarium. <http://www.mhi.co.jp/enews/e_0898.html>, 2001 (accessed October 2007).
[25] D. Barrett, RoboTuna I, Massachusetts Institute of Technology. <http://web.mit.edu/towtank/www/Tuna/tuna.html>, 1995 (accessed October 2007).
[26] D. Beal, M. Sachinis, RoboTuna II, Massachusetts Institute of Technology. <http://web.mit.edu/towtank/www/Tuna/Tuna2/tuna2.html>, 2000 (accessed October 2007).
[27] K. Hirata, D. Aoki, Prototype Fish Robot, PF-200, National Maritime Research Institute. <http://www.nmri.go.jp/eng/khirata/fish/experiment/pf200/index_e.html>, 2003 (accessed October 2007).

[28] K.H. Low, Parametric study of modular and reconfigurable robotic fish with caudal fin mechanisms, in: Proceedings of the 2007 IEEE International Conference on Mechatronics and Automation (ICMA 2007), Heilongjiang, China, 2007, pp. 123–128.
[29] <http://www.aquascuba.net/photo_gallery.htm> (accessed October 2007).
[30] M. Epstein, J.E. Colgate, M.A. MacIver, Generating thrust with a biologically-inspired robotic ribbon fin, in: Proceedings of the IEEE/RSJ International Conference on Intelligent Robots and Systems (IROS06), Beijing, China, 2006, pp. 2412–2417.
[31] Y. Toda, N. Sogihara, Y. Sanada, M. Danno, The motion of a fish-like under-water vehicle with two undulating side fins, in: Proceedings of the Third International Symposium on Aero Aqua Bio-mechanisms (ISABMEC06), Okinawa, Japan, 2006.
[32] K.H. Low, A. Willy, Biomimetic motion planning of an undulating robotic fish fin, Journal of Vibration and Control 12 (12) (2006) 1337–1359.
[33] M.J. Lighthill, Note on the swimming of slender fish, Journal of Fluid Mechanics 9 (1960) 305–317.
[34] K.H. Low, Mechatronics and buoyancy implementation of robotic fish with modular fin mechanisms, Proceedings of the Institution of Mechanical Engineers (Proc. IMechE), Part I: Journal of Systems and Control Engineering 221 (3) (2007) 295–309.
[35] K.H. Low, Maneuvering of biomimetic fish by integrating a buoyancy body with modular undulating fins, International Journal of Humanoid Robotics 4 (4) (2007) 671–695.
[36] K.A. Harper, M.D. Berkemeier, S. Grace, Decreasing the energy costs of swimming robots through the passive elastic elements, in: Proceedings of the 1997 IEEE International Conference on Robotics and Automation, Albuquerque, New Mexico, 1997, pp. 1839–1844.
[37] G. Dogangil, E. Ozcicek, A. Kuzucu, Modeling, simulation, and development of a robotic dolphin prototype, in: Proceedings of the IEEE International Conference on Mechatronics and Automation (ICMA05), Niagara Falls, Canada, 2005, pp. 952–957.
[38] P. Miller, The genius of swarms, National Geographic 212 (1) (2007) 126–147.
[39] K.H. Low, A comprehensive approach for the eigenproblem of beams with arbitrary boundary conditions, Computers and Structures 39 (6) (1991) 671–678.
[40] K.H. Low, Solution schemes for the system equations of flexile robots, Journal of Robotic Systems 6 (4) (1989) 383–405.
[41] K.H. Low, An equivalent-centre-weight factor method for predicting fundamental frequencies of plates carrying multiple masses from experimental test data, Journal of Sound and Vibration 168 (1) (1993) 123–139.
[42] Z. Wang et al, A micro-robot fish with embedded SMA wire actuated flexible biomimetic fin, Sensors and Actuators A: Physical 144 (2) (2008) 354–360.
[43] K.H. Low, et al., Initial prototype design and investigation of an undulating body by SMA, in: Proceedings of the IEEE International Conference on Automation Science and Engineering (CASE2006), Shanghai, China, 2006, pp. 472–477.
[44] W. Zhang, S.-X. Guo, K. Asaka, A new type of hybrid fish-like microrobot, International Journal of Automation and Computing 4 (2006) 365–385.